# Rainfall erosivity in subtropical catchments and implications for erosion and particle-bound contaminant transfer: a case-study of the Fukushima region

J. P. Laceby, C. Chartin, O. Evrard, Y. Onda, L. Garcia-Sanchez, O. Cerdan

Hydrol. Earth Syst. Sci. Discuss., 12, 7225–7266, 2015
www.hydrol-earth-syst-sci-discuss.net/12/7225/2015/
doi:10.5194/hessd-12-7225-2015


Hydrology and Earth System Sciences
Open Access
Discussions



# Rainfall erosivity in subtropical catchments and implications for erosion and particle-bound contaminant transfer: a case-study of the Fukushima region

**J. P. Laceby[1], C. Chartin[2], O. Evrard[1], Y. Onda[3], L. Garcia-Sanchez[4], and O. Cerdan[5]**

[1]Laboratoire des Sciences du Climat et de l'Environnement (LSCE), Unité Mixte de Recherche 8212 (CEA-CNRS-UVSQ/IPSL), Gif-sur-Yvette, France
[2]Georges Lemaître Centre for Earth and Climate Research, Earth and Life Institute, Université Catholique de Louvain, Louvain, Belgium
[3]Graduate School of Life and Environmental Sciences, Center for Research in Isotopes and Environmental Dynamics (CRIED), University of Tsukuba, Tsukuba, Japan
[4]Laboratoire de Biogéochimie, Biodisponibilité et Transferts de Radionucléides, IRSN/PRP-ENV/SERIS/L2BT, Cadarache, France
[5]Bureau de Recherches Géologiques et Minières, Orléans, France







Received: 10 July 2015 – Accepted: 11 July 2015 – Published: 30 July 2015

Correspondence to: J. P. Laceby (placeby@lsce.ipsl.fr)

Published by Copernicus Publications on behalf of the European Geosciences Union.







## Abstract

The Fukushima Dai-ichi nuclear power plant (FDNPP) accident in March 2011 resulted in a significant fallout of radiocesium over the Fukushima region. After reaching the soil surface, radiocesium is almost irreversibly bound to fine soil particles. Thereafter, rainfall and snow melt run-off events transfer particle-bound radiocesium downstream. Erosion models, such as the Universal Soil Loss Equation (USLE), depict a proportional relationship between rainfall and soil erosion. As radiocesium is tightly bound to fine soil and sediment particles, characterizing the rainfall regime of the fallout-impacted region is fundamental to modelling and predicting radiocesium migration. Accordingly, monthly and annual rainfall data from ~60 meteorological stations within a 100 km radius of the FDNPP were analysed. Monthly rainfall erosivity maps were developed for the Fukushima coastal catchments illustrating the spatial heterogeneity of rainfall erosivity in the region. The mean average rainfall in the Fukushima region was 1387 mm $yr^{-1}$ ($\sigma$ 230) with the mean rainfall erosivity being 2785 MJ mm $ha^{-1}$ $yr^{-1}$ ($\sigma$ 1359). The results indicate that the majority of rainfall (60 %) and rainfall erosivity (86 %) occurs between June and October. During the year, rainfall erosivity evolves positively from northwest to southeast in the eastern part of the prefecture, whereas a positive gradient from north to south occurs in July and August, the most erosive months of the year. During the typhoon season, the coastal plain and eastern mountainous areas of the Fukushima prefecture, including a large part of the contamination plume, are most impacted by erosive events. Understanding these rainfall patterns, particularly their spatial and temporal variation, is fundamental to managing soil and particle-bound radiocesium transfers in the Fukushima region. Moreover, understanding the impact of typhoons is important for managing sediment transfers in subtropical regions impacted by cyclonic activity.





HESSD
12, 7225–7266, 2015



## 1 Introduction

In March 2011, the great Tohuku earthquake triggered a giant tsunami that resulted in the Fukushima Dai-ichi nuclear power plant (FDNPP) release of the largest amount of radioactive material since Chernobyl (Chino et al., 2011; Thakur et al., 2013; Steinhauser, 2014). After the decay of short-lived radionuclides initially present in the fallout (e.g. $^{131}$I, $^{110m}$Ag, $^{129}$Te), the radionuclide with the most serious short and long-term human health concerns is radiocesium ($t_{1/2}$ $^{134}$Cs – 2 yr; $^{137}$Cs – 30 yr) (Kitamura et al., 2014; Saito et al., 2015).

Radiocesium is rapidly bound to fine soil particles and remains stored within the top 0–5 cm of the soil profile (He and Walling, 1996; Tamura, 1964; Sawhiney, 1972; He and Walling, 1997; Kato et al., 2012). As radiocesium is fixated to soil particles in the upper layer of the soil profile, soil erosion and particle transport processes are considered to be the main processes transferring radiocesium downstream (Saito and Onda, 2015; Evrard et al., 2015; Yamashiki et al., 2014).

Rainfall drives erosion by detaching particles from the soil surface, primarily through the kinetic energy of raindrops (Wischmeier and Smith, 1958; Renard and Freimund, 1994; Moore, 1979). The potential of rainfall to erode soils is referred to as rainfall erosivity (Mello et al., 2013; Vrieling et al., 2014). Understanding rainfall erosivity is fundamental to determining the climatic vulnerability of a region, like Fukushima, to rainfall-driven soil erosion (Mello et al., 2013).

The Universal Soil Loss Equation (USLE) (Wischmeier and Smith, 1978) and its revised edition (RUSLE) (Renard et al., 1997) represent one of the most broadly adopted soil erosion modelling frameworks (Oliveira et al., 2013). The wide adoption of the USLE is based on its' relatively simple modelling framework that predicts average annual soil loss with six factors pertaining to soil, topography, vegetation, management and rainfall erosivity, or the *R* factor.

The *R* factor is one of the main variables in the (R)USLE, quantifying the climatic influence of rainfall to erode soil (Lee and Heo, 2011; Lu and Yu, 2002; Wischmeier





HESSD
12, 7225–7266, 2015



and Smith, 1958). When all other soil erosion factors in the (R)USLE are held constant, there is a proportional relationship between soil loss and the *R* factor (Yu and Rosewell, 1996; Lu and Yu, 2002; Shamshad et al., 2008; Wischmeier and Smith, 1958, 1978).

The *R* factor estimates rainfall erosivity as a combined function of event duration and intensity (Diodato and Bellocchi, 2010). It sums all storm erosion values individually calculated through multiplying each storm's total kinetic energy with its maximum measured 30 min rainfall intensity (Agnese et al., 2006; Wischmeier and Smith, 1978). To incorporate cyclical rainfall variations, the *R* factor is averaged over long temporal periods (~ 20 years) (Renard and Freimund, 1994; Wischmeier and Smith, 1978).

The *R* factor is considered one of the better predictors of the potential erosivity of rainfall (de Santos Loureiro and de Azevedo Coutinho, 2001; Stocking and Elwell, 1976). At many research sites around the world, the *R* factor has been found to be highly correlated to soil loss (Ferro et al., 1999; Renard and Freimund, 1994; Wischmeier and Smith, 1958, 1978). The utility of the *R* factor is reflected in its' global application (McFarlane et al., 1986; Ma et al., 2014; Vrieling et al., 2014).

There are limitations with the application of the *R* factor and the USLE (Kinnell, 2010; Brooks et al., 2014). The USLE is designed to model soil erosion on a 22.1 m × 5 m plot over ~ 20 years (Wischmeier and Smith, 1978). Although the USLE was originally conceptualized within a plot-scale framework, the approach is often incorporated in catchment scale research (Wilkinson et al., 2009; Kitamura et al., 2014; Belyaev et al., 2005). Further, it is important to combine rainfall erosivity layers with a cover factor that seasonally depicts soil erodibility based on land cover (Evrard et al., 2010). A debate on the applicability of the USLE within catchment scale modelling frameworks is beyond the scope of this current research. What is important is that the *R* factor and a thorough characterization of the rainfall regime are fundamental to understanding soil erosion and riverine particulate transfers, particularly in subtropical catchments subject to cyclonic activity.

The goal of this research was to improve the understanding of soil and radiocesium transfers in a subtropical climate affected by typhoons. As improved estimates of rainfall





HESSD
12, 7225–7266, 2015



erosivity result in more accurate modelling results (Renard et al., 1991; Lee and Heo, 2011), a comprehensive examination of rainfall erosivity will provide a concrete foundation for building a better understanding of sediment and radiocesium behaviour in the Fukushima region. Accordingly, this research thoroughly characterizes rainfall (38–120 years of daily rainfall data) and rainfall erosivity (19 years of 10 min data) in the Fukushima region. Importantly, this research provides rainfall erosivity maps (monthly and annual) for the Fukushima region along with rainfall erosivity data for all events selected by the RUSLE criteria (see Supplement).

## 2 Methods

### 2.1 Study area

Most of the terrestrial fallout from the FDNPP accident occurred over the coastal catchments of the Fukushima Prefecture (Fig. 1). The region has a humid, subtropical climate along the Pacific coast (Cwa in the Köppen–Geiger climate classification; Peel et al., 2007), transitioning to a humid continental climate (Dfa) progressing westward. Based on these classifications, the westward continental region has large differences in seasonal temperatures with hot and humid summers and cold winters. The subtropical coastal region has slightly warmer winters, along with hot humid summers and more rainfall in the summer months compared to relatively dry winters. In comparison, the region most directly affected by the Chernobyl fallout predominantly has a humid continental climate (Dfb). The main difference between the climate of these fallout-affected regions is the typhoon driven precipitation in the Fukushima region that results in high volumes and intensities of rainfall occurring during extreme events between July and October (Evrard et al., 2015, 2014; Chartin et al., 2013).





HESSD
12, 7225–7266, 2015



## 2.2 Rainfall monitoring stations

All rainfall stations within a 100 km radius of the FDNPP were selected along with two additional long-term stations within 115 km (Fig. 1). From this initial selection, all rainfall stations that recorded pluviometric data consistently (e.g. throughout the entire year) for more than five years were selected for preliminary analyses (Table 1). There were 14 stations omitted within the 100 km radius of the FDNPP, five stations because they had less than five years of data, and another nine stations that were not operational during winter. Up to 19 years was available for the 10 min rainfall data (1995–2013) and 38 years for daily rainfall data (1976–2013) for the majority of the rainfall stations. Four long-term stations had daily rainfall data for over 100 years.

The rainfall stations are operated by the Japan Meteorological Agency's (JMA) Automated Meteorological Data Acquisition System (AMeDAS). All rainfall data were downloaded directly from the JMA website (http://www.jma.go.jp/jma/index.html). For the daily data, there were on average 45 stations recording daily rainfall data consistently between 1977 and 2013, including the long-term rainfall stations. The total number of stations recording daily rainfall data varied from 32 stations in 1977 to 48 for multiple years after 2003. The variation in "live" stations results from different initiation dates for the daily rainfall recordings. As only 12 rainfall stations were operational in 1976 (less than a quarter of the stations analyzed), this year was omitted from the analysis. The minimum duration of the long-term stations was 60 years with a maximum of 126 years. These long-term stations were included in the analysis of daily rainfall starting from 1977. Further, all daily rainfall data from the long-term stations was also analyzed separately to investigate potential long-term rainfall trends.

For the 10 min data, there were on average 38 stations operating consistently between 1995 and 2013. As the $R$ factor is a parameter of long-term rainfall erosivity (e.g. $\sim$ 20 years), only stations with 10 min rainfall data for over 10 years were included in the initial analyses. The main difference between number of stations utilized in the daily and 10 min analyses was that the long-term stations did not start recording 10 min





HESSD
12, 7225–7266, 2015



data until August 2008 along with two other stations that had less than 10 years of 10 min data (Table 2). Most stations (88 %) had 19 years of 10 min data. In total, 40 stations were used to derive $R$ factor data with an average of 38 per year. For both daily and 10 min data, station 300 was not operational after the FDNPP accident in 2011 coming back online late in 2012. Accordingly, data from 2011 for this station was omitted for these analyses.

### 2.3 $R$ factor calculations

The Rainfall Intensity Summarisation Tool (RIST) software (USDA, 2013) was used to calculate the $R$ factor, which is a product of the kinetic energy (KE) of an individual rainfall event ($E$) and its maximum 30 min intensity ($I_{30}$) (Renard and Freimund, 1994):

$$R = \frac{1}{n}\sum_{j=1}^{n}\sum_{k=1}^{mj}(EI_{30})_k \quad (1)$$

where $R$ equals the annual average rainfall erosivity in MJ mm ha$^{-1}$ h$^{-1}$ yr$^{-1}$, $n$ represents the number of years of rainfall data utilized, $m_j$ is the number of erosive rainfall events in year $j$, and $EI_{30}$ was calculated as:

$$EI_{30} = \left(\sum_{r=1}^{0} e_r v_r\right) I_{30} \quad (2)$$

with $e_r$ representing the unit rainfall energy in MJ mm ha$^{-1}$ h$^{-1}$, $v_r$ is the volume of rainfall (mm) during a given time interval ($r$), and $I_{30}$ is the maximum rainfall intensity over a 30 min period of the rainfall event (mm h$^{-1}$). For each time interval, the unit of rainfall energy ($e_r$) was calculated as:

$$e_r = 0.29[1 - 0.72^{(-0.05i_r)}] \quad (3)$$





HESSD
12, 7225–7266, 2015



with $i_r$ being the rainfall intensity for the time interval (mm h$^{-1}$) (Renard and Freimund, 1994).

To calculate the annual and monthly $R$ factors, erosive rainfall events ($m_j$) were summed for each monitoring station for the considered period (months or year). The criteria of Renard et al. (1997) were used to define an erosive event, where: (1) cumulative rainfall of the given event is > 12.7 mm, or (2) the rainfall event has, at minimum, one peak which is > 6.35 mm over a 15 min period (or 12.7 mm over a 30 min period), (3) rainfall accumulations < 1.27 mm over a 6 h period splits rainfall events into two different periods, and (4) a 12.7 mm threshold is applied to identify rainfall events with erosive potential.

The $R$ factor for each rainfall station was calculated with and without temperature control to account for potential impacts of snowfall. For example, when the temperature dropped below 0 °C, any precipitation that occurred was considered to be snowfall and thus not included in erosivity calculations for $R$ factor calculations with temperature control. For all sites with temperature data, the $R$ factor was calculated with and without temperature control to examine the potential impact of snowfall on rainfall erosivity. Throughout the results and discussion, the term rainfall is used even though it may incorporate some precipitation that occurred as snowfall in the winter.

### 2.4 *R* factor spatial analyses

Annual and monthly $R$ factor data were used to derive maps of annual and monthly rainfall erosivity over the eastern part of the Fukushima Prefecture. A regression approach based on relationships established between rainfall erosivity and spatially-distributed covariates was used to produce these maps. The covariates used for the spatial interpolation of annual and monthly $R$ factors over the study area were:

– Elevation from a Digital Elevation Model (DEM) of the eastern part of the Fukushima Prefecture with a 10 m resolution provided by the Geospatial Information Authority of Japan (GSI) from the Ministry of Land, Infrastructure, Transport





HESSD
12, 7225–7266, 2015



and Tourism (http://www.gsi.go.jp/). This DEM was derived from LIDAR airborne monitoring surveys. Different derivatives were computed based on this DEM: slope, aspect along with eastness and northness, which represent the degree to which aspect is close to the east and the north, respectively (Zar, 2010).

- Climatic data, i.e. monthly mean rainfall and temperature, from the WorldClim database reported for the period 1950–2000 (30 arcsec resolution, equivalent to 1 km resolution) (Hijmans et al., 2005).

- Geographical coordinates (longitude and latitude) of the stations in order to include spatial autocorrelation.

A spatial resolution of 40 m was chosen as a compromise between spatial resolution and computation time. Continuous variables were rescaled in ArcGIS10 (ESRI, 2011) with bilinear interpolation, which determined the output value of a cell based on a weighted distance average of the four nearest input cell centres.

The spatial variation of monthly and annual *R* factors was modeled with Generalized Additive Models (GAM; Hastie and Tibshirani, 1986), implemented in the mgcv package in R (Wood, 2001). The GAM regression technique is a generalization of linear regression models in which the coefficients may be a set of smoothing functions, accounting for the non-linearity that may exist between the dependent variable and covariates. This regression technique was chosen to (i) create erosivity maps (i.e. proceed to spatial interpolation) and (ii) examine which explanatory covariates influence the spatial variation of rainfall erosivity annually and month after month in the eastern part of Fukushima prefecture. Moreover, the GAM technique is more straightforward and flexible in comparison to the other approaches to spatial interpolation of rainfall data, i.e. kriging and co-kriging.

A Generalized Additive Model was fitted for each month and for annual observations of 38 of the 40 stations used for *R* factor calculation. The southernmost station (1011; Fig. 1) was rejected from the dataset because its location at the boundary of the area covered by the DEM layer. Station 326, located at the SW of the study area (Fig. 1),





HESSD
12, 7225–7266, 2015



was consistently an outlier for most of the months and years examined. There may be a significant change in climatic conditions occurring in this direction or more likely, different climatic conditions dominating locally, resulting from the presence of a nearby volcano. The goodness-of-fit of most of the models was significantly improved within the study area by not including station 326 (results not shown). Hence, this station was rejected from the dataset used for the mapping procedure.

GAM specifies a distribution for the conditional mean $\mu(Y)$ and a link function, $g$, relating to an additive function of the covariates:

$$g[\mu(Y)] = \alpha + f_1 X_1 + f_2 X_2 + \cdots + f_p X_p \quad (4)$$

where $Y$ is the dependent variable, $X_1$, $X_2$, ... $X_p$ represent the covariates and the $f_i$'s the smooth (non-parametric) functions.

A Gaussian error model incorporated the conditional mean $\mu$ ($Y$) and, due to the predominant logarithmic distribution of the monthly and annual data, a log-linear link function $g(\mu) = \log(\mu)$ was incorporated. The GAM models were built using regression splines fitted by penalized Maximum Likelihood to avoid over-fitting. For each month and the year, a model including all the covariates was developed. Next, a backward stepwise procedure was applied to select the appropriate covariates: sequentially omitting the covariate with the highest non-significant $p$ value from the model and re-fitting until all remaining covariates were significant, as indicated in Wood (2001). The level of significance was set at $p < 0.01$. The deviances explained were calculated and compared for each model created during this procedure. Then, a Bayesian approach, as proposed in the mgcv package, was used to compute standard errors and confidence intervals for the predictions. To finish, a leave-one-out cross-validation procedure was applied to each fitted model: the mean error (ME) was calculated to indicate if the prediction was biased and the mean absolute error (MAE) was used to measure the accuracy of the model.





HESSD
12, 7225–7266, 2015



## 3 Results

### 3.1 Spatial and temporal rainfall variability

Rainfall in the Fukushima region varies spatially. Based on daily rainfall data from 1977–2013, the mean annual rainfall ranged from a minimum of 1069 mm yr$^{-1}$ (station 47592) to a maximum of 2184 mm yr$^{-1}$ (station 1116) (Table 1). The mean annual rainfall for 49 stations and their standard deviation (error bars) is plotted in rank order in Fig. 2 along with the mean (solid line – 1387 mm) and standard deviation (dashed line $\sigma$ 230 mm) for all stations analysed. The coefficient of variation for the daily rainfall was 17 %, with 22 % ($n$ = 11) of the rainfall stations plotting outside one standard deviation on the mean, indicative of spatial heterogeneous rainfall in the Fukushima region.

The annual temporal variation in rainfall for the Fukushima region is illustrated in Fig. 3. Between 1977 and 2013, the minimum mean annual rainfall was 855 mm (1984) compared to a maximum of 1819 mm (2006). The coefficient of variance for the annual rainfall was 15 %. Almost a quarter of the years (24 %, $n$ = 9) plotted outside one standard deviation on the mean, indicative of temporally variable rainfall.

This temporal variation in annual rainfall was maintained over a longer temporal period (Fig. 4). For the long-term stations, the mean annual rainfall over the 124 year period was 1249 mm yr$^{-1}$ ($\sigma$ 117 mm) with a 9 % coefficient of variation. The 10 year rolling average for these long-term stations demonstrates that the region experiences prolonged wet/dry periods that last approximately 15–25 years. Of note, these long-term rainfall stations plot near ($n$ = 2), or below ($n$ = 5) the annual rainfall mean for all of the stations, and they therefore may not be indicative of all rainfall trends in the region (Fig. 2).

Rainfall in the Fukushima region varies monthly. The majority of rainfall occurs during the summer months and early into fall coinciding with a summer wet season that includes periodic typhoons (Fig. 5). In fact, 60 % of the rainfall occurred between June and October, compared to only 17 % between November and February. The remaining 22 % of the annual precipitation was recorded in spring (March–May). Among the rain-





HESSD
12, 7225–7266, 2015



fall stations, there was additional spatial variation in the monthly rainfall. For example, the maximum monthly average was 322 mm at site 1116 in July compared to 147 mm for site 47592 in September.

Variation was also evident in the mean maximum daily rainfall in the Fukushima region (Fig. 6). The highest maximum daily rainfall recorded was 607 mm in 1998 at Site 326, compared to the lowest maximum daily rainfall of 38 mm in 1984 at site 294. The mean maximum daily rainfall was 112 mm ($\sigma$ 26 mm). The highest annual maximum daily rainfall (169 mm) was recorded in 2011 compared to a minimum of 61 mm in 1984. Although the daily rainfall maximum is not an optimal indicator of rainfall depth owing to the probability of rainfall events occurring over multiple days, the year of the FDNPP accident, 2011, had the highest daily maximum rainfall (169 mm) over this analysis period (1977–2013).

### 3.2 Spatial and temporal *R* factor variability

Before examining spatial and temporal variations in rainfall erosivity, it is important to understand the influence of snowfall on the *R* factor to determine which rainfall stations can be included in the analyses. In the region, 29 rainfall stations simultaneously recorded rainfall and temperature. The difference in the *R* factor between these stations after removing precipitation that occurred when the temperature was below 0 °C, was less than 1 %. The mean difference was 4.7 MJ mm ha$^{-1}$ yr$^{-1}$ ($\sigma$ 10.5). The maximum difference between *R* factor calculations was only 2.2 % (42.4 MJ mm ha$^{-1}$ yr$^{-1}$). Therefore, all rainfall stations that did not record temperature ($n$ = 11) were included in the following *R* factor analyses as no significant difference ($t$ test $p$: 0.495) was found with the exclusion of precipitation that may have fallen as snow.

As the *R* factor is calculated from rainfall, it also varied spatially and temporally. All following *R* factor values are in MJ mm ha$^{-1}$ yr$^{-1}$. The maximum annual *R* factor was 8575 (site 326) compared to a minimum of 1169 (site 290). A rank order plot of the mean annual *R* factor and standard deviation for rainfall stations is plotted in Fig. 2 along with the mean annual *R* factor ($\mu$ 2785) and standard deviation ($\sigma$ 1359)





HESSD
12, 7225–7266, 2015



for all stations. The coefficient of variation for the $R$ factor across the stations was 49 %, almost three times the variation of the annual average rainfall indicating that rainfall erosivity is more spatially variable than rainfall. This variability is largely driven by site 326 which is the only station plotting above one standard deviation of the rainfall erosivity mean, while 4 stations plot below. The percent of stations plotting outside 1 standard deviation of the rainfall erosivity mean is 15 %, a 7 % decrease from total rainfall, with this decrease likely driven by site 326.

In the Fukushima region, the annual $R$ factor varied temporally, similarly to the annual precipitation, with the exceptions of 2003 and 2005 (Fig. 3). The mean annual $R$ factor ranged from a maximum of 5817 in 1998 to a minimum of 1356 in 1996. The mean average annual $R$ factor and standard deviation are plotted in Fig. 3 along with the individual standard deviations (error bars) for each rainfall station. The coefficient of variation for the annual $R$ factors was 40 %. Just over a quarter of years (26 %, $n = 5$) plotted outside one standard deviation of the mean, similar to the 24 % for the rainfall variation.

The highest monthly $R$ factors occurred in the summer months and early fall coinciding with the wet summer and typhoon season (Fig. 5). In fact, 86 % of the rainfall erosivity occurs between June and October in the Fukushima region, an increase of 16 % compared to the amount of rainfall during this period. In particular, 68 % of the rainfall erosivity occurs between July and September. Winter (November–February) only contributes 4.6 % of the total annual $R$ factor with spring (March–May) contributing the remaining 9.9 %.

### 3.3 Spatial and temporal distribution of rainfall erosivity

Annual and monthly $R$ factors were mapped through fitting of GAM models to selected environmental covariates leading to the development of 13 models. Predicted values for the 38 rain stations showed similar distributions to the observed values (Table 3) for the year and for the months between October and May. For the months between June and September, which include the wet and typhoon seasons, the standard deviations





HESSD
12, 7225–7266, 2015



of simulated values were smaller than the observed values. The corresponding models tended to overestimate lower values and underestimate higher values. The deviance explained by the models was relatively good to very good varying from 67 % for August to 98 % for April, and 81 % for the annual *R* factor.

The mean errors (ME) calculated by the leave-one-out cross validation procedure were close to zero ($-1 < \mathrm{ME} < 1$) for models depicting *R* factors from November to March. Models for the months of April to October showed a slight positive bias ranging from 1.2 to 7.7 $\mathrm{MJ\,mm\,ha^{-1}\,h^{-1}\,month^{-1}}$, except for the month of September which showed a slight negative bias of $-1.9\ \mathrm{MJ\,mm\,ha^{-1}\,h^{-1}\,month^{-1}}$. These biases remained relatively low considering corresponding observed values and their variability. The mean error for the annual model was of 26.5 $\mathrm{MJ\,mm\,ha^{-1}\,h^{-1}\,yr^{-1}}$. The mean absolute error (MAE) ranged from 2.8 $\mathrm{MJ\,mm\,ha^{-1}\,h^{-1}\,month^{-1}}$ for February to 180.0 $\mathrm{MJ\,mm\,ha^{-1}\,h^{-1}\,month^{-1}}$ for August, varying according to observed *R* factor values and variability. The MAE was 469.9 $\mathrm{MJ\,mm\,ha^{-1}\,h^{-1}\,yr^{-1}}$ for the annual model.

The computed map for the annual *R* factor and the errors relative to the model are presented in Fig. 7. The backward stepwise procedure selected the projected coordinates, the mean monthly rainfalls of June, September and October, and the slope to model the spatial variation of annual *R* factor in the eastern Fukushima Prefecture. The annual *R* factor is positively correlated to precipitation of these three months, showing a similar spatial distribution (Fig. 7a), i.e. a predominantly positive gradient from northwest to southeast with a second positive gradient related to elevation. Moreover, the annual *R* factor rises with slopes from lowlands to mountainous areas. It is important to consider that few stations are located in areas where elevation and slope gradient are greater than 600 m and 20 %, respectively. Consequently, the modeling error is most pronounced in these areas (e.g. Fig. 7b), when elevation and slope are selected as explanatory covariates during the modeling procedure. These steep mountainous areas are mainly forested and likely have limited export of eroded soils.

The backward stepwise procedure selected the projected coordinates for all months of the year. *R* factors are spatially distributed according to a dominant gradient which





HESSD
12, 7225–7266, 2015



direction evolves during the year (Fig. 8). Whereas *R* factors arises predominantly from northwest to southeast from September to June, it evolves positively from north to south during the rainfall season (i.e. the most erosive months of July and August). During the typhoon season, the coastal plain and eastern mountainous areas of the Fukushima Prefecture, including the FDNPP and a large part of the contamination plume, appear to be the most impacted by significant erosive events.

In addition to the coordinates, the explanatory covariates selected varied over the year (Table 4). The most selected were slope and eastness amongst the morphometric covariates, and monthly mean precipitation for the climatic covariates. Only morphometric covariates were additionally selected for the winter months of January and February. From March to May, some morphometric and climatic parameters explained the *R* factor variance. During June to August, only climatic parameters helped to describe the *R* factor spatial distribution whereas during September and October climatic and morphometric covariates were again selected. To finish, only slope was selected additionally to coordinates to model monthly *R* factor distribution for November, whereas only climatic covariates were selected for the month of December. Monthly *R* factors showed more equivalent relationships with monthly mean precipitations and slopes than the annual *R* factor. The selection of eastness demonstrated that rainfall erosivity appears more efficient on hillslopes oriented E to SE. The maps of standard errors related to the models of monthly *R* factors are available in the Supplement (Fig. S1).

## 4 Discussion

### 4.1 Rainfall

As the Fukushima region transitions from a humid, subtropical climate along the Pacific coast to a humid continental climate progressing inland, spatial variation in rainfall is expected. The cyclical nature of the rainfall in the coastal region, resulting from the location and intensity of seasonal typhoon events likely drives the spatial and temporal





HESSD
12, 7225–7266, 2015



variation in rainfall. Long-term climatic oscillations (e.g., El Niño) potentially influence the weather patterns illustrated by the 10 year rolling average reported in the long-term analyses.

The mean annual temperature in the Fukushima region is 11.3 °C ($\sigma$ 1.7) ranging from a mean of 0.0 ($\sigma$ 2.1) in January to 23.4 ($\sigma$ 1.4) in August. The average rainfall in the Fukushima region (1387 mm) is ~ 300 mm less than the mean annual precipitation in Japan (1684 mm) (Kim et al., 2010). Along the western and southeast coast of Japan, annual precipitation may be greater than 3000 mm (Kim et al., 2010). In the southeast of Japan, the elevated annual rainfall is related to an increasingly tropical climate progressing southwards and the increased occurrence of typhoons in these warmer climates with higher rainfall intensities during summer months.

Intra-annual rainfall variability in the Fukushima study area directly reflects the region's location on a climatic transition between humid continental and humid subtropical coastal climates. The significant monthly variation in rainfall clearly indicates that the majority of rainfall occurs in the summer months, likely the result of the high humidity and residual influences of the seasonal typhoon activity progressing inland.

The climate of the Chernobyl region in Ukraine similarly classifies as a humid continental climate. Although the climates are technically similar in classification, Ukraine receives significantly less precipitation than the Fukushima region. For example in the Kharkiv region, the mean annual precipitation is 460 mm (Nazarok et al., 2014). Odessa also has a mean annual precipitation less than 500 mm (Svetlitchnyi, 2009). Importantly, the Chernobyl region does not have cyclonic activity in the summer, resulting in the higher maximum daily and summer rainfall observed in the Fukushima region. The difference in climate between these two regions could result in faster wash-off of the initial radiocesium fallout, a deeper penetration of radiocesium in soils, and potentially a quicker transfer of higher quantities of radiocesium downstream.





HESSD
12, 7225–7266, 2015



### 4.2 *R* factor

Similarly to annual precipitation, rainfall erosivity varied spatially and temporally in the Fukushima region. Rainfall erosivity is known to vary in other regions of the world, including the Mediterranean region (Capolongo et al., 2008) and the Middle East (Eltaif et al., 2010). Although researchers have demonstrated relationships between rainfall and the *R* Factor (Ma et al., 2014), in the Fukushima region the relationship was positive, though not significant ($r^2$ 0.39). The lack of significant relationship was likely the result of the *R* factor varying more than rainfall itself. The most pronounced variation for the *R* factor was temporal, with 5 years having an *R* factor less than 2000 compared to 6 years where it was greater than 3000. There are also possibly decadal *R* factor variations, similarly to rainfall, that require long-term analyses to confirm.

Across the Fukushima region and Japan, there have been a range of *R* factors reported. This range may reflect spatial–temporal variations in the *R* factor itself, or possibly differences in approaches used to quantify or report the *R* factor. Yoshimura et al. (2015) calculated an *R* factor of 3413 in the Fukushima area, nearly 25 % greater than this current research.

Around Japan a variety of *R* factors have been reported, for example 5880 in the Onga River basin (Fukuoka prefecture – South Japan) (Tran et al., 2011), 4568 in the Shiraska River catchment (Aichi prefecture – Central Japan) (Karki and Shibano, 2006), and 2890 in the Hirose River catchment (Miyagi prefecture – Northern Japan) (Takeuchi and Ishidaira, 2001). Shiono et al. (2013) found that rainfall erosivity varied from 721 to 35 299 across Japan with a mean of 5130. In our current analyses, rainfall erosivity in the Fukushima region was found to be similar to the results of Shiono et al. (2013) who spatially depicted rainfall erosivity in the Fukushima region being between 2500 and 5000.

Shiono et al. (2013) also demonstrated that rainfall erosivity in the Fukushima region is relatively low compared to the rest of Japan. Similarly to annual precipitation, there is a rainfall erosivity gradient in Japan from north to south, particularly along the Pacific





HESSD
12, 7225–7266, 2015



coast with rainfall erosivity increasing southwards from the colder temperate/subarctic regions in the north towards the tropical regions in the south. Importantly, the rainfall erosivity of the Fukushima region is projected, by Shiono et al. (2013), to increase significantly as a result of climate change.

Carvalho (1994) modified a classification table for rainfall erosivity (Table 5) that has also been integrated into rainfall erosivity research in a Himalayan catchment (Ma et al., 2014). According to this classification, rainfall erosivity in the Fukushima region (2785) is described as medium erosivity. This classification reflects the transition from a temperate to subtropical climate in the region.

Tropical regions subject to typhoons have much higher rainfall erosivity. In Mexico, the mean annual rainfall erosivity was 6525 (García-Oliva et al., 1995). In Peninsular Malaysia, the *R* factor was shown to range between 9000 and 14 000 (Shamshad et al., 2008) in one study and between 1360 and 21 600 in another (Yu et al., 2001). Comparatively, arid regions have lower rainfall erosivity. In Jordan, rainfall erosivity was reported to be between 86 and 779 (Eltaif et al., 2010) and in South Australia rainfall erosivity was found to vary mostly between 250 and 500 (Yu and Rosewell, 1996).

There is a paucity of rainfall erosivity data for Ukraine. For the European region, the mean rainfall erosivity was reported to be 722 (Panagos et al., 2015). Ukraine, particularly the non-coastal regions would be expected to have an *R* factor of less than 1000, or 2.7 times less than in the Fukushima region. As there is a direct proportional relationship between rainfall erosivity and soil loss, where other factors are held equal, it would be anticipated that there would be double the erosion and concomitant radiocesium transfer in the Fukushima region compared to Chernobyl.

### 4.3 Typhoons

In regions subject to tropical cyclones or typhoons, the majority of the annual precipitation and rainfall erosivity may be derived from only a few storms (García-Oliva et al., 1995). Often, several large and intense rainfall events mobilize and transport the largest proportion of sediment (Angulo-Martínez and Beguería, 2009). Tropical storms





HESSD
12, 7225–7266, 2015



result in high intensity rainfall over a particular region and likely drive the spatial and temporal variation in the rainfall and rainfall erosivity in the Fukushima region. In fact, typhoon activity may be fundamental to determining which years have high rainfall erosivity (García-Oliva et al., 1995). Accordingly, modelling erosion in the Fukushima region may be effective in the short term by incorporating the frequency and occurrence of major events and examining the $EI_{30}$ of major events and their runoff frequency (Chartin et al., 2015).

### 4.4 Snow control

In other regions around the world with higher volumes of snowfall, the inclusion of temperature controls may have a significant impact on the *R* factor. In the Fukushima region, the majority of precipitation occurs in the summer months making the temperature control on the *R* factor less important. The inclusion of temperature control likely did not make a significant difference owing to the dominance of the coastal climate. Further, it would take significant volumes of snowfall to be calculated in the *R* factor as in general there is a 10 : 1 depth ratio between snow and liquid rainfall equivalent. Although this general relationship is subject to multiple complex factors that may alter this ratio, it simply illustrates that significant snowfall events are required to be incorporated into the *R* factor calculations (e.g. > 120.7 mm of snow). In the Fukushima region, there is likely insufficient liquid equivalent in snow fall events to be incorporated into the *R* factor. Nonetheless, researchers have documented a runoff snowmelt transfer of radiocesium throughout the coastal catchments (Evrard et al., 2014; Lepage et al., 2014).

### 4.5 Implications and limitations

The *R* factor maps demonstrate that areas most contaminated with radiocesium with the highest rainfall erosivity are located along the coast of the Pacific Ocean north west of the FDNPP. Catchments in these areas will have the highest susceptibility to rainfall





HESSD
12, 7225–7266, 2015



induced soil erosion and concomitant radiocesium transfers to downstream catchments and ultimately to the Pacific Ocean. The highest precipitation in these areas occurs during the typhoon season (July–September).

So far, research on radiocesium and sediment transfers in the Fukushima region has focused on modelling and monitoring without a comprehensive examination of rainfall erosivity. Accordingly, up-to-date and Fukushima up-to-date *R* factor maps are provided online (database link to be provided) for use in on-going modelling work in the Fukushima region. Further, all the rainfall event data are included in the Supplement (Table S1). Although there are many approaches to modelling the influence of rainfall on erosivity, we believe the provision of the *R* factor maps and a thorough quantification of the rainfall erosivity in the Fukushima region is beneficial to the research and management community.

To effectively incorporate rainfall erosivity into catchment modelling, it is necessary to quantify the variation in the seasonal erodibility of rice paddy fields and other land covers in the Fukushima region. Indeed, incorporating the interaction between rainfall erosivity and landscape cover is fundamental to accurately predicting soil erosion (Evrard et al., 2010). Understanding this interaction is even more important in subtropical climates subject to intense typhoons such as the Fukushima region.

## 5 Conclusions

Rainfall erosivity in the Fukushima region is characterized as medium (2785 $MJ\,mm\,ha^{-1}\,h^{-1}$) and the region receives on average 1387 mm of rainfall per year. Although these are below average values for Japan, they are more than 2-fold higher than in Chernobyl. It is mainly the occurrence of major typhoon events in the summer that is responsible for the elevated rainfall in the Fukushima region. The majority of rainfall (60 %) and rainfall erosivity (86 %) occurs between June and October.





HESSD
12, 7225–7266, 2015



Owing to the increasing requirement for modelling and understanding radiocesium transfers in the Fukushima region, spatial maps of the *R* factor have been generated. Understanding this variation will contribute to the design of appropriate measures to manage sediment transfers, and importantly the related radiocesium transfers from hillslopes to the Pacific Ocean. This research also provides insight into the impact of typhoons on rainfall erosivity and the importance for the incorporation of this driver of soil erosion when examining sediment and particle-bound contaminant transfers in subtropical regions subject to cyclonic activity.

**The Supplement related to this article is available online at doi:10.5194/hessd-12-7225-2015-supplement.**

*Author contributions.* J. P. Laceby and L. Garcia-Sanchez downloaded and prepared the data, J. P. Laceby and C. Chartin performed the analyses, all authors were fundamental to drafting and editing the manuscript.

*Acknowledgements.* This research was funded by the ANR (French National Research Agency) in the framework of the AMORAD project (ANR-11-RSNR-0002).

## References

Agnese, C., Bagarello, V., Corrao, C., D'Agostino, L., and D'Asaro, F.: Influence of the rainfall measurement interval on the erosivity determinations in the Mediterranean area, J. Hydrol., 329, 39–48, doi:10.1016/j.jhydrol.2006.02.002, 2006.

Angulo-Martínez, M. and Beguería, S.: Estimating rainfall erosivity from daily precipitation records: A omparison among methods using data from the Ebro Basin (NE Spain), J. Hydrol., 379, 111–121, doi:10.1016/j.jhydrol.2009.09.051, 2009.

Belyaev, V. R., Golosov, V. N., Ivanova, N. N., Markelov, M. V., and Tishkina, E. V.: Human-accelerated soil redistribution within an intensively cultivated dry valley catchment in southern European Russia, IAHS-AISH P., 291, 11–20, 2005.





HESSD
12, 7225–7266, 2015



Brooks, A., Spencer, J., Borombovits, D., Pietsch, T., and Olley, J.: Measured hillslope erosion rates in the wet-dry tropics of Cape York, northern Australia: Part 2, RUSLE-based modeling significantly over-predicts hillslope sediment production, Catena, 122, 1–17, doi:10.1016/j.catena.2014.06.002, 2014.

Capolongo, D., Diodato, N., Mannaerts, C. M., Piccarreta, M., and Strobl, R. O.: Analyzing temporal changes in climate erosivity using a simplified rainfall erosivity model in Basilicata (southern Italy), J. Hydrol., 356, 119–130, doi:10.1016/j.jhydrol.2008.04.002, 2008.

Chartin, C., Evrard, O., Onda, Y., Patin, J., Lefèvre, I., Ottlé, C., Ayrault, S., Lepage, H., and Bonté, P.: Tracking the early dispersion of contaminated sediment along rivers draining the Fukushima radioactive pollution plume, Anthropocene, 1, 23–34, 2013.

Chartin, C., Evrard, O., Onda, Y., Laceby, P., Cerdan, O., Lepage, H., Ottlé, C., Lefèvre, I., and Bonté, P.: The impact of typhoons on sediment connectivity: lessons learnt from contaminated coastal catchments of Fukushima Prefecture (Japan), Earth Surf. Proc. Land., in review, 2015.

Chino, M., Nakayama, H., Nagai, H., Terada, H., Katata, G., and Yamazawa, H.: Preliminary estimation of release amounts of $^{131}$I and $^{137}$Cs accidentally discharged from the Fukushima Daiichi nuclear power plant into the atmosphere, J. Nucl. Sci. Technol., 48, 1129–1134, 2011.

de Santos Loureiro, N. and de Azevedo Coutinho, M.: A new procedure to estimate the RUSLE EI30 index, based on monthly rainfall data and applied to the Algarve region, Portugal, J. Hydrol., 250, 12–18, doi:10.1016/S0022-1694(01)00387-0, 2001.

Diodato, N. and Bellocchi, G.: MedREM, a rainfall erosivity model for the Mediterranean region, J. Hydrol., 387, 119–127, doi:10.1016/j.jhydrol.2010.04.003, 2010.

Eltaif, N. I., Gharaibeh, M. A., Al-Zaitawi, F., and Alhamad, M. N.: Approximation of rainfall erosivity factors in north Jordan, Pedosphere, 20, 711–717, doi:10.1016/S1002-0160(10)60061-6, 2010.

ESRI: ArcGIS Desktop: Release 10, Environmental Systems Research Institute, Redlands, CA, 2011.

Evrard, O., Nord, G., Cerdan, O., Souchère, V., Le Bissonnais, Y., and Bonté, P.: Modelling the impact of land use change and rainfall seasonality on sediment export from an agricultural catchment of the northwestern European loess belt, Agr. Ecosyst. Environ., 138, 83–94, 2010.





HESSD
12, 7225–7266, 2015



Evrard, O., Chartin, C., Onda, Y., Lepage, H., Cerdan, O., Lefevre, I., and Ayrault, S.: Renewed soil erosion and remobilisation of radioactive sediment in Fukushima coastal rivers after the 2013 typhoons, Sci. Rep., 4, 4574, doi:10.1038/srep04574, 2014.

Evrard, O., Laceby, J. P., LePage, H., Onda, Y., Cerdan, O., and Ayrault, S.: Radiocesium transfer from hillslopes to the Pacific Ocean after the Fukushima Nuclear Power Plant accident: a review, J. Environ. Radioactiv., 148, 92–110, doi:10.1016/j.jenvrad.2015.06.018, 2015.

Ferro, V., Porto, P., and Yu, B.: A comparative study of rainfall erosivity estimation for southern Italy and southeastern Australia, Hydrolog. Sci. J., 44, 3–24, doi:10.1080/02626669909492199, 1999.

García-Oliva, F., Maass, J. M., and Galicia, L.: Rainstorm analysis and rainfall erosivity of a seasonal tropical region with a strong cyclonic influence on the Pacific coast of mexico, J. Appl. Meteorol., 34, 2491–2498, doi:10.1175/1520-0450(1995)034<2491:RAAREO>2.0.CO;2, 1995.

Hastie, T. and Tibshirani, R.: Generalized additive models, Stat. Sci., 1, 297–310, 1986.

He, Q. and Walling, D. E.: Interpreting particle size effects in the adsorption of $^{137}$Cs and unsupported $^{210}$Pb by mineral soils and sediments, J. Environ. Radioactiv., 30, 117–137, doi:10.1016/0265-931X(96)89275-7, 1996.

He, Q. and Walling, D. E.: The distribution of fallout $^{137}$Cs and $^{210}$Pb in undisturbed and cultivated soils, Appl. Radiat. Isotopes, 48, 677–690, 1997.

Hijmans, R. J., Cameron, S. E., Parra, J. L., Jones, P. G., and Jarvis, A.: Very high resolution interpolated climate surfaces for global land areas, Int. J. Climatol., 25, 1965–1978, 2005.

Karki, K. B. and Shibano, H.: Soil loss in a forested watershed underlain by deeply weathered granite: comparison of observations to predictions of a GIS-based USLE, Bull. Tokyo Univ. Forests, 115, 1–36, 2006.

Kato, H., Onda, Y., and Teramage, M.: Depth distribution of $^{137}$Cs, $^{134}$Cs, and $^{131}$I in soil profile after Fukushima Dai-ichi nuclear power plant accident, J. Environ. Radioactiv., 111, 59–64, doi:10.1016/j.jenvrad.2011.10.003, 2012.

Kim, S., Nakakita, E., Tachikawa, Y., and Takara, K.: Precipitation changes in Japan under the A1B climate change scenario, Annual J. Hydraul. Eng. ASCE, 54, 127–132, 2010.

Kinnell, P. I. A.: Event soil loss, runoff and the Universal Soil Loss Equation family of models: a review, J. Hydrol., 385, 384–397, doi:10.1016/j.jhydrol.2010.01.024, 2010.





HESSD
12, 7225–7266, 2015



Kitamura, A., Yamaguchi, M., Kurikami, H., Yui, M., and Onishi, Y.: Predicting sediment and cesium-137 discharge from catchments in eastern Fukushima, Anthropocene, 5, 22–31, doi:10.1016/j.ancene.2014.07.001, 2014.
Lee, J.-H. and Heo, J.-H.: Evaluation of estimation methods for rainfall erosivity based on annual precipitation in Korea, J. Hydrol., 409, 30–48, doi:10.1016/j.jhydrol.2011.07.031, 2011.
Lepage, H., Evrard, O., Onda, Y., Chartin, C., Ayrault, S., and Bonté, P.: Tracking the Origin and Dispersion of Contaminated Sediments Transported by Rivers Draining the Fukushima Radioactive Contaminant Plume Sediment Dynamics from the Summit to the Sea, IAHS Publ. 367, Proceedings of a symposium held in New Orleans, 11–14 December 2014, Louisiana, USA, 237–243, doi:10.5194/piahs-367-237-2015, 2014.
Lu, H. and Yu, B.: Spatial and seasonal distribution of rainfall erosivity in Australia, Soil Research, 40, 887–901, 2002.
Ma, X., He, Y., Xu, J., van Noordwijk, M., and Lu, X.: Spatial and temporal variation in rainfall erosivity in a Himalayan watershed, Catena, 121, 248–259, doi:10.1016/j.catena.2014.05.017, 2014.
McFarlane, D., Westcott, T., and Davies, J.: Rainfall erosivity in Western Australia, in: 17th Hydrology and Water Resources Symposium, Brisbane, Qld., Institution of Engineers, Australia, Barton, ACT, 350–354, 1986.
Mello, C. R., Viola, M. R., Beskow, S., and Norton, L. D.: Multivariate models for annual rainfall erosivity in Brazil, Geoderma, 202–203, 88–102, doi:10.1016/j.geoderma.2013.03.009, 2013.
Moore, T.: Rainfall erosivity in East Africa, Geogr. Ann. A, 61, 147–156, 1979.
Nazarok, P., Kruglov, O., Menshov, O., Kutsenko, M., and Sukhorada, A.: Mapping soil erosion using magnetic susceptibility. A case study in Ukraine, Solid Earth Discuss., 6, 831–848, doi:10.5194/sed-6-831-2014, 2014.
Oliveira, P. T. S., Wendland, E., and Nearing, M. A.: Rainfall erosivity in Brazil: a review, Catena, 100, 139–147, doi:10.1016/j.catena.2012.08.006, 2013.
Panagos, P., Ballabio, C., Borrelli, P., Meusburger, K., Klik, A., Rousseva, S., Tadić, M. P., Michaelides, S., Hrabaliková, M., and Olsen, P.: Rainfall erosivity in Europe, Sci. Total Environ., 511, 801–814, 2015.
Peel, M. C., Finlayson, B. L., and McMahon, T. A.: Updated world map of the Köppen-Geiger climate classification, Hydrol. Earth Syst. Sci., 11, 1633–1644, doi:10.5194/hess-11-1633-2007, 2007.





HESSD
12, 7225–7266, 2015



Renard, K. G. and Freimund, J. R.: Using monthly precipitation data to estimate the *R* factor in the revised USLE, J. Hydrol., 157, 287–306, doi:10.1016/0022-1694(94)90110-4, 1994.
Renard, K. G., Foster, G. R., Weesies, G. A., and Porter, J. P.: RUSLE: revised universal soil loss equation, J. Soil Water Conserv., 46, 30–33, 1991.
Renard, K. G., Foster, G. R., Weesies, G. A., McCool, D., and Yoder, D.: Predicting soil erosion by water: a guide to conservation planning with the revised universal soil loss equation (RUSLE), Agriculture Handbook No. 703, US Department of Agriculture, Washington, D.C., 404 pp., 1997.
Saito, K. and Onda, Y.: Outline of the national mapping projects implemented after the Fukushima accident, J. Environ. Radioactiv., 139, 240–249, 2015.
Saito, K., Tanihata, I., Fujiwara, M., Saito, T., Shimoura, S., Otsuka, T., Onda, Y., Hoshi, M., Ikeuchi, Y., and Takahashi, F.: Detailed deposition density maps constructed by large-scale soil sampling for gamma-ray emitting radioactive nuclides from the Fukushima Dai-ichi Nuclear Power Plant accident, J. Environ. Radioactiv., 139, 308–319, 2015.
Sawhiney, B.: Selective sorption and fixation of cations by clay minerals: a review, Clay. Clay Miner., 20, 93–100, 1972.
Shamshad, A., Azhari, M. N., Isa, M. H., Hussin, W. M. A. W., and Parida, B. P.: Development of an appropriate procedure for estimation of RUSLE EI30 index and preparation of erosivity maps for Pulau Penang in Peninsular Malaysia, Catena, 72, 423–432, doi:10.1016/j.catena.2007.08.002, 2008.
Shiono, T., Ogawa, S., Miyamoto, T., and Kameyama, K.: Expected impacts of climate change on rainfall erosivity of farmlands in Japan, Ecol. Eng., 61, 678–689, 2013.
Steinhauser, G.: Fukushima's forgotten radionuclides: a review of the understudied radioactive emissions, Environ. Sci. Technol., 48, 4649–4663, doi:10.1021/es405654c, 2014.
Stocking, M. and Elwell, H.: Rainfall erosivity over Rhodesia, T. I. Brit. Geogr., 1, 231–245, 1976.
Svetlitchnyi, A.: Soil erosion induced degradation of agrolandscapes in Ukraine: modeling, computation and prediction in conditions of the climate changes, in: Regional Aspects of Climate–Terrestrial–Hydrologic Interactions in Non-boreal Eastern Europe, NATO Science for Peace and Security Series C: Environmental Security, edited by: Groisman, P. and Ivanov, S., Springer, the Netherlands, 191–199, doi:10.1007/978-90-481-2283-7_21, 2009.
Takeuchi, B. K. and Ishidaira, H.: The examination of sediment production estimation by the USLE method in mountainous basins of Japan, Hydraul. Eng., 45, 85–90, 2001.





HESSD
12, 7225–7266, 2015



Tamura, T.: Consequences of activity release: selective sorption reactions of cesium with soil minerals, Nucl. Safety, 5, 262–268, 1964.
Thakur, P., Ballard, S., and Nelson, R.: An overview of Fukushima radionuclides measured in the Northern Hemisphere, Sci. Total Environ., 458–460, 577–613, doi:10.1016/j.scitotenv.2013.03.105, 2013.
Tran, T. A., Mitani, Y., Ikemi, H., and Matsuki, H.: Human impacts on erosion and deposition in Onga River basin, Kyushu, Japan, Memoirs of the Faculty of Engineering, Kyushu University, 71, 47–65, 2011.
USDA: Rainfall Intensity Summarization Tool (RIST), Version 3.88, United States Department of Agriculture (USDA), Agriculture Research Service, National Sedimentation Laboratory, Oxford, MS, 2013.
Vrieling, A., Hoedjes, J. C. B., and van der Velde, M.: Towards large-scale monitoring of soil erosion in Africa: accounting for the dynamics of rainfall erosivity, Global Planet. Change, 115, 33–43, doi:10.1016/j.gloplacha.2014.01.009, 2014.
Wilkinson, S. N., Prosser, I. P., Rustomji, P., and Read, A. M.: Modelling and testing spatially distributed sediment budgets to relate erosion processes to sediment yields, Environ. Modell. Softw., 24, 489–501, 2009.
Wischmeier, W. H. and Smith, D. D.: Rainfall energy and its relationship to soil loss, T. Am. Geophys. Un., 39, 285–291, doi:10.1029/TR039i002p00285, 1958.
Wischmeier, W. H. and Smith, D. D.: Predicting Rainfall Erosion Losses – a Guide to Conservation Planning, Agriculture Handbooks USA No. 537, United States Department of Agriculture (USDA), Washington, D.C., 1978.
Wood, S. N.: mgcv: GAMs and generalized ridge regression for R, R News, 1, 2–25, 2001.
Yamashiki, Y., Onda, Y., Smith, H. G., Blake, W. H., Wakahara, T., Igarashi, Y., Matsuura, Y., and Yoshimura, K.: Initial flux of sediment-associated radiocesium to the ocean from the largest river impacted by Fukushima Daiichi nuclear power plant, Scient. Reports, 4, 3714, doi:10.1038/srep03714, 2014.
Yoshimura, K., Onda, Y., and Kato, H.: Evaluation of radiocaesium wash-off by soil erosion from various land uses using USLE plots, J. Environ. Radioactiv., 139, 362–369, doi:10.1016/j.jenvrad.2014.07.019, 2015.
Yu, B. and Rosewell, C.: Rainfall erosivity estimation using daily rainfall amounts for South Australia, Soil Research, 34, 721–733, doi:10.1071/SR9960721, 1996.





HESSD
12, 7225–7266, 2015



Yu, B., Hashim, G., and Eusof, Z.: Estimating the *R* factor with limited rainfall data: a case study from peninsular Malaysia, J. Soil Water Conserv., 56, 101–105, 2001.
Zar, J. H.: Biostatistical Analysis, 5th Edn., Prentice Hall, New Jersey, 944 pp., 2010.





HESSD
12, 7225–7266, 2015



**Table 1.** Rainfall stations in the Fukushima region analyzed for spatial and temporal trends in daily rainfall.

| Station | Latitude | Longitude | Start | Finish | Complete Years | Missing Data (%) | Mean Annual Rainfall (mm) | SD (Annual Rainfall mm) |
|---|---|---|---|---|---|---|---|---|
| 254 | 38.178 | 140.635 | 15 Apr 1976 | 26 Oct 2005 | 28 | 0.25 | 1429 | 302 |
| 256 | 38.015 | 140.612 | 15 Apr 1976 | 31 Dec 2013 | 37 | 0.05 | 1285 | 247 |
| 257 | 38.025 | 140.858 | 15 Apr 1976 | 31 Dec 2013 | 37 | 0.05 | 1250 | 265 |
| 279 | 37.912 | 140.143 | 1 Jan 1976 | 31 Dec 2013 | 38 | 0.67 | 1336 | 218 |
| 281 | 37.852 | 140.588 | 7 Dec 1976 | 31 Dec 2013 | 37 | 0.12 | 1092 | 173 |
| 285 | 37.783 | 140.925 | 1 Jan 1976 | 31 Dec 2013 | 37 | 0.21 | 1336 | 265 |
| 288 | 37.638 | 140.983 | 1 Jan 1976 | 31 Dec 2013 | 37 | 0.03 | 1319 | 271 |
| 290 | 37.552 | 140.108 | 30 Nov 1976 | 31 Dec 2013 | 37 | 0.10 | 1272 | 247 |
| 291 | 37.583 | 140.430 | 13 Apr 1976 | 31 Dec 2013 | 37 | 0.24 | 1173 | 225 |
| 294 | 37.435 | 140.577 | 14 Apr 1976 | 31 Dec 2013 | 37 | 0.12 | 1158 | 210 |
| 295 | 37.492 | 140.965 | 20 Apr 1976 | 31 Dec 2013 | 37 | 0.29 | 1482 | 302 |
| 299 | 37.368 | 140.330 | 1 Jan 1976 | 31 Dec 2013 | 37 | 0.06 | 1157 | 179 |
| 300 | 37.347 | 141.017 | 1 Jan 1976 | 14 Mar 2011 | 34 | 0.15 | 1522 | 301 |
| 304 | 37.287 | 140.625 | 1 Jan 1976 | 31 Dec 2013 | 37 | 0.38 | 1232 | 204 |
| 307 | 37.147 | 140.460 | 16 Apr 1976 | 31 Dec 2013 | 34 | 0.11 | 1278 | 201 |
| 310 | 37.065 | 140.877 | 16 Apr 1976 | 31 Dec 2013 | 34 | 2.90 | 1391 | 298 |
| 312 | 36.938 | 140.408 | 17 Apr 1976 | 31 Dec 2013 | 37 | 0.06 | 1402 | 237 |
| 314 | 36.868 | 140.637 | 1 Jan 1976 | 31 Dec 2013 | 38 | 0.19 | 1993 | 381 |
| 315 | 36.833 | 140.772 | 1 Jan 1976 | 31 Dec 2013 | 38 | 0.33 | 1472 | 251 |
| 316 | 36.778 | 140.345 | 14 Mar 1977 | 31 Dec 2013 | 36 | 0.13 | 1417 | 199 |
| 326 | 37.123 | 140.035 | 1 Jan 1976 | 31 Dec 2013 | 38 | 0.45 | 1962 | 379 |
| 1011 | 36.580 | 140.645 | 1 Jan 1976 | 31 Dec 2013 | 38 | 0.04 | 1474 | 235 |
| 1034 | 37.233 | 141.000 | 12 Apr 1976 | 31 Dec 2013 | 37 | 0.27 | 1564 | 284 |
| 1116 | 37.668 | 140.260 | 27 Apr 1994 | 31 Dec 2013 | 19 | 0.44 | 2184 | 367 |
| 1127 | 37.008 | 140.737 | 30 Nov 1976 | 16 Mar 2009 | 32 | 0.17 | 1435 | 285 |
| 1129 | 37.337 | 140.808 | 30 Nov 1976 | 31 Dec 2013 | 37 | 0.32 | 1426 | 244 |
| 1130 | 37.695 | 140.747 | 4 Dec 1976 | 31 Dec 2013 | 37 | 0.21 | 1295 | 245 |
| 1132 | 38.003 | 140.207 | 19 Apr 1977 | 31 Dec 2013 | 36 | 0.37 | 1255 | 199 |
| 1150 | 37.560 | 140.753 | 24 Mar 1977 | 31 Dec 2013 | 37 | 0.89 | 1324 | 235 |
| 1173 | 36.778 | 140.482 | 16 Jul 1977 | 31 Dec 2013 | 37 | 0.03 | 1431 | 233 |
| 1220 | 37.932 | 140.778 | 5 Nov 1977 | 31 Dec 2013 | 36 | 0.07 | 1253 | 248 |
| 1268 | 37.288 | 140.218 | 20 Apr 1979 | 31 Dec 2013 | 34 | 0.02 | 1366 | 262 |
| 1274 | 37.207 | 140.750 | 5 Apr 1979 | 31 Dec 2013 | 34 | 0.15 | 1427 | 273 |
| 1282 | 37.722 | 140.058 | 28 Oct 1978 | 31 Dec 2013 | 35 | 0.60 | 1771 | 317 |
| 1293 | 37.892 | 140.437 | 21 Dec 1978 | 31 Dec 2013 | 35 | 0.46 | 1363 | 180 |
| 1294 | 37.277 | 140.063 | 1 Nov 1978 | 31 Dec 2013 | 35 | 0.57 | 1556 | 284 |
| 1298 | 37.827 | 140.728 | 23 Apr 1979 | 31 Dec 2013 | 34 | 0.07 | 1449 | 272 |
| 1386 | 37.388 | 140.090 | 19 Jun 1982 | 31 Dec 2013 | 31 | 0.10 | 1315 | 237 |
| 1421 | 36.743 | 140.593 | 6 Jun 1985 | 31 Dec 2013 | 28 | 0.20 | 1841 | 284 |
| 1464 | 38.138 | 140.917 | 1 Jan 2003 | 31 Dec 2013 | 11 | 0.31 | 1121 | 189 |
| 1466 | 37.227 | 140.427 | 1 Jan 2003 | 31 Dec 2013 | 11 | 0.02 | 1230 | 226 |
| 1564 | 38.127 | 140.680 | 28 Oct 2005 | 31 Dec 2013 | 8 | 0.19 | 1328 | 179 |
| 47570 | 37.488 | 139.910 | 1 Aug 1953 | 31 Dec 2013 | 60 | 28.42 | 1197 | 212 |
| 47588 | 38.255 | 140.345 | 1 Jul 1889 | 31 Dec 2013 | 124 | 30.88 | 1170 | 177 |
| 47590 | 38.262 | 140.897 | 1 Oct 1926 | 31 Dec 2013 | 87 | 33.15 | 1257 | 226 |
| 47592 | 38.427 | 141.298 | 1 Sep 1887 | 31 Dec 2013 | 126 | 41.83 | 1069 | 169 |
| 47595 | 37.758 | 140.470 | 1 May 1889 | 31 Dec 2013 | 125 | 34.86 | 1155 | 207 |
| 47597 | 37.132 | 140.215 | 1 Jan 1940 | 31 Dec 2013 | 74 | 34.55 | 1406 | 266 |
| 47598 | 36.947 | 140.903 | 1 May 1910 | 31 Dec 2013 | 103 | 47.45 | 1412 | 223 |





HESSD
12, 7225–7266, 2015



**Table 2.** Rainfall erosivity results for rainfall stations in the Fukushima region analyzed for spatial and temporal trends in daily rainfall.

| Station | Lat. | Long. | Start | Finish | Temp | Complete Years | Missing Data (%) | Mean Annual KE ($MJ\,ha^{-1}$) | $EI_{30}$ ($MJ\,mm\,ha^{-1}\,h^{-1}$) |
|---|---|---|---|---|---|---|---|---|---|
| 254 | 38.178 | 140.635 | 1 Jan 1995 | 26 Oct 2005 | Yes | 10 | 0.16 | 84 | 2051 |
| 256 | 38.015 | 140.612 | 1 Jan 1995 | 31 Dec 2013 | Yes | 19 | 0.24 | 72 | 1469 |
| 257 | 38.025 | 140.858 | 1 Jan 1995 | 31 Dec 2013 | Yes | 19 | 0.16 | 76 | 1895 |
| 279 | 37.912 | 140.143 | 20 Jun 2006 | 31 Dec 2013 | Yes | 8 | – | – | – |
| 281 | 37.852 | 140.588 | 1 Jan 1995 | 31 Dec 2013 | Yes | 19 | 0.44 | 55 | 1213 |
| 285 | 37.783 | 140.925 | 1 Jan 1995 | 31 Dec 2013 | Yes | 19 | 0.12 | 92 | 2653 |
| 288 | 37.638 | 140.983 | 1 Jan 1995 | 31 Dec 2006 | No | 19 | 0.10 | 168 | 3610 |
| 290 | 37.552 | 140.108 | 1 Jan 1995 | 31 Dec 2013 | Yes | 19 | 0.19 | 55 | 1169 |
| 291 | 37.583 | 140.430 | 1 Jan 1995 | 31 Dec 2013 | Yes | 19 | 0.07 | 65 | 1501 |
| 294 | 37.435 | 140.577 | 1 Jan 1995 | 31 Dec 2013 | Yes | 19 | 0.16 | 70 | 1673 |
| 295 | 37.492 | 140.965 | 1 Jan 1995 | 31 Dec 2013 | Yes | 19 | 0.62 | 110 | 3035 |
| 299 | 37.368 | 140.330 | 1 Jan 1995 | 31 Dec 2013 | Yes | 19 | 0.35 | 67 | 1689 |
| 300 | 37.347 | 141.017 | 1 Jan 1995 | 31 Dec 2013 | No | 17 | 10.73 | 203 | 4290 |
| 304 | 37.287 | 140.625 | 1 Jan 1995 | 31 Dec 2013 | Yes | 19 | 0.14 | 76 | 2086 |
| 307 | 37.147 | 140.460 | 1 Jan 1995 | 31 Dec 2013 | Yes | 19 | 0.35 | 82 | 2317 |
| 310 | 37.065 | 140.877 | 1 Jan 1995 | 31 Dec 2013 | No | 19 | 0.83 | 110 | 3037 |
| 312 | 36.938 | 140.408 | 1 Jan 1995 | 31 Dec 2013 | Yes | 19 | 0.14 | 106 | 3197 |
| 314 | 36.868 | 140.637 | 1 Jan 1995 | 31 Dec 2013 | No | 19 | 0.34 | 168 | 5307 |
| 315 | 36.833 | 140.772 | 1 Jan 1995 | 31 Dec 2013 | Yes | 19 | 0.84 | 104 | 2834 |
| 316 | 36.778 | 140.345 | 1 Jan 1995 | 31 Dec 2013 | Yes | 19 | 0.22 | 115 | 3868 |
| 326 | 37.123 | 140.035 | 1 Jan 1995 | 31 Dec 2013 | Yes | 19 | 0.13 | 280 | 8575 |
| 1011 | 36.580 | 140.645 | 1 Jan 1995 | 31 Dec 2013 | Yes | 19 | 0.18 | 110 | 3166 |
| 1034 | 37.233 | 141.000 | 1 Jan 1995 | 31 Dec 2013 | Yes | 19 | 0.44 | 118 | 3147 |
| 1116 | 37.668 | 140.260 | 1 Jan 1995 | 31 Dec 2013 | Yes | 19 | 0.54 | 133 | 3330 |
| 1127 | 37.008 | 140.737 | 1 Jan 1995 | 16 Mar 2009 | Yes | 14 | 0.35 | 101 | 2491 |
| 1129 | 37.337 | 140.808 | 1 Jan 1995 | 31 Dec 2013 | Yes | 19 | 0.51 | 97 | 2674 |
| 1130 | 37.695 | 140.747 | 1 Jan 1995 | 31 Dec 2013 | Yes | 19 | 0.31 | 77 | 1800 |
| 1132 | 38.003 | 140.207 | 1 Jan 1995 | 31 Dec 2013 | Yes | 19 | 0.31 | 57 | 1616 |
| 1150 | 37.560 | 140.753 | 1 Jan 1995 | 31 Dec 2013 | No | 19 | 0.24 | 161 | 3440 |
| 1173 | 36.778 | 140.482 | 1 Jan 1995 | 31 Dec 2013 | No | 19 | 0.18 | 112 | 3168 |
| 1220 | 37.932 | 140.778 | 1 Jan 1995 | 31 Dec 2013 | Yes | 19 | 0.22 | 74 | 1858 |
| 1268 | 37.288 | 140.218 | 1 Jan 1995 | 31 Dec 2013 | No | 19 | 0.16 | 91 | 2656 |
| 1274 | 37.207 | 140.750 | 1 Jan 1995 | 31 Dec 2013 | No | 19 | 0.11 | 177 | 4000 |
| 1282 | 37.722 | 140.058 | 1 Jan 1995 | 31 Dec 2013 | Yes | 19 | 0.16 | 86 | 2108 |
| 1293 | 37.892 | 140.437 | 1 Jan 1995 | 31 Dec 2013 | Yes | 19 | 0.23 | 65 | 1490 |
| 1294 | 37.277 | 140.063 | 1 Jan 1995 | 31 Dec 2013 | Yes | 19 | 0.23 | 95 | 2643 |
| 1298 | 37.827 | 140.728 | 1 Jan 1995 | 31 Dec 2013 | No | 19 | 0.18 | 172 | 3560 |
| 1386 | 37.388 | 140.090 | 1 Jan 1995 | 31 Dec 2013 | No | 19 | 0.08 | 68 | 1849 |
| 1421 | 36.743 | 140.593 | 1 Jan 1995 | 31 Dec 2013 | No | 19 | 0.64 | 152 | 4804 |
| 1464 | 38.138 | 140.917 | 1 Jan 2003 | 31 Dec 2013 | Yes | 11 | 0.68 | 70 | 1916 |
| 1466 | 37.227 | 140.427 | 1 Jan 2003 | 31 Dec 2013 | Yes | 11 | 0.34 | 80 | 2173 |
| 1564 | 38.127 | 140.680 | 27 Oct 2005 | 31 Dec 2013 | Yes | 8 | – | – | – |
| 47570 | 37.488 | 139.910 | 25 Jun 2008 | 31 Dec 2013 | Yes | 5 | – | – | – |
| 47588 | 38.255 | 140.345 | 25 Jun 2008 | 31 Dec 2013 | Yes | 5 | – | – | – |
| 47590 | 38.262 | 140.897 | 25 Jun 2008 | 31 Dec 2013 | Yes | 5 | – | – | – |
| 47592 | 38.427 | 141.298 | 25 Jun 2008 | 31 Dec 2013 | Yes | 5 | – | – | – |
| 47595 | 37.758 | 140.470 | 25 Jun 2008 | 31 Dec 2013 | Yes | 5 | – | – | – |
| 47597 | 37.132 | 140.215 | 25 Jun 2008 | 31 Dec 2013 | Yes | 5 | – | – | – |
| 47598 | 36.947 | 140.903 | 25 Jun 2008 | 31 Dec 2013 | Yes | 5 | – | – | – |





HESSD
12, 7225–7266, 2015



**Table 3.** Observed and predicted means and standard deviations of monthly and annual $R$ factors (in $MJ\,mm\,ha^{-1}\,h^{-1}\,yr^{-1}$ for annual $R$ factor and in $MJ\,mm\,ha^{-1}\,h^{-1}\,month^{-1}$ for monthly $R$ factors), and parameters describing performance of GAM models used to map $R$ factors in the area. (GAM models were fitted in a data from a total of 38 rain stations).

| Month or Year | Observed $R$ | | Predicted $R$ | | Deviance explained (%) | Model performance | |
|---|---|---|---|---|---|---|---|
| | Mean | SD* | Mean | SD* | | ME | MAE |
| Year | 2559.56 | 1016.59 | 2553.24 | 928.63 | 81.3 | 6.32 | 467.4 |
| January | 21.64 | 22.93 | 20.80 | 21.56 | 96.0 | 0.42 | 10.49 |
| February | 7.20 | 7.00 | 7.48 | 6.52 | 83.6 | −0.28 | 3.58 |
| March | 21.82 | 21.49 | 21.89 | 17.84 | 80.0 | −0.07 | 11.12 |
| April | 91.80 | 82.62 | 92.08 | 69.22 | 93.5 | −0.28 | 47.48 |
| May | 132.53 | 131.06 | 126.97 | 118.61 | 96.9 | 5.56 | 60.55 |
| June | 198.38 | 104.15 | 201.09 | 87.11 | 69.8 | −2.70 | 61.99 |
| July | 605.76 | 221.74 | 601.88 | 176.80 | 65.4 | 3.88 | 137.06 |
| August | 577.54 | 250.11 | 569.11 | 197.22 | 64.7 | 8.43 | 152.42 |
| September | 560.66 | 222.96 | 553.52 | 187.15 | 76.6 | 7.45 | 120.10 |
| October | 250.74 | 204.98 | 250.87 | 190.80 | 94.5 | −0.13 | 66.97 |
| November | 34.62 | 26.93 | 34.82 | 23.10 | 87.8 | −0.20 | 14.50 |
| December | 56.87 | 65.96 | 56.48 | 58.66 | 93.5 | 0.43 | 38.79 |

* Standard Deviation





HESSD
12, 7225–7266, 2015



**Table 4.** Covariates selected by backward stepwise procedure for the map computation in addition to projected coordinates. The numbers correspond to the importance of the parameters as explanatory covariates (determined by the degree of change of the deviance explained value when the concerned covariate is dropped from the model).

| Month | Morphometric covariates | | | | | Climatic covariates | |
|---|---|---|---|---|---|---|---|
| | Elevation | Slope | Aspect | Eastness | Northness | Monthly mean precipitation | Monthly mean temperature |
| January | | X | | X | | | |
| February | X | X | | X | | | |
| March | | X | | | | X | |
| April | | X | | | X | X | X |
| May | | X | | X | | X | |
| June | | | | | | X | |
| July | | | | | | X | |
| August | | | | | | | X |
| September | | X | X | | | X | |
| October | | X | | | | X | |
| November | | X | | | | | |
| December | | | | | | X | X |





HESSD
12, 7225–7266, 2015



**Table 5.** Erosivity Ranking.

| Rank | $EI_{30}$ ($MJ\,mm^{-1}\,ha^{-1}\,h^{-1}$) |
|---|---|
| Low erosivity | < 2452 |
| Medium erosivity | 2452–4905 |
| Medium-strong erosivity | 4905–7357 |
| Strong erosivity | 7357–9810 |
| Very strong erosivity | > 9810 |

Source: Carvalho (1994).





HESSD
12, 7225–7266, 2015



**Table A1. Dataset 1**: *R* factor Maps in ArcGis Raster (grid) format (40 m) will be provided. We are currently searching for an archiving/database service online to host the 13 Map files (1 for each month and the annual maps) as the size of the maps is much greater than the ~ 50 mb HESS limit. **Dataset 2**: Table of rainfall data results for all events included in the analyses (an example of the databased to be appended including 20 000 events over the study period for rainfall stations analyzed is provided below).

| Stn | sRecord | eRecord | sYYYY | sMM | sDD | sHH | smm | eYYYY | eMM | eDD | eHH | emm | toRain | KE | IE30 | *R* |
|---|---|---|---|---|---|---|---|---|---|---|---|---|---|---|---|---|
| 254 | 3103 | 3145 | 1995 | 1 | 22 | 13 | 40 | 1995 | 1 | 22 | 20 | 40 | 17 | 1.9 | 4 | 7.6 |
| 254 | 9895 | 10 010 | 1995 | 3 | 10 | 17 | 40 | 1995 | 3 | 11 | 12 | 50 | 58.5 | 7 | 7 | 49.3 |
| 254 | 10 766 | 10 808 | 1995 | 3 | 16 | 18 | 50 | 1995 | 3 | 17 | 1 | 50 | 17.5 | 2 | 4 | 7.9 |
| 254 | 12 728 | 12 846 | 1995 | 3 | 30 | 9 | 50 | 1995 | 3 | 31 | 5 | 30 | 69 | 9.2 | 10 | 92.1 |
| 254 | 19 001 | 19 122 | 1995 | 5 | 12 | 23 | 20 | 1995 | 5 | 13 | 19 | 30 | 88.5 | 13.7 | 18 | 246 |
| 254 | 19 533 | 19 593 | 1995 | 5 | 16 | 16 | 0 | 1995 | 5 | 17 | 2 | 0 | 23 | 3 | 9 | 27.1 |
| 254 | 22 119 | 22 207 | 1995 | 6 | 3 | 15 | 0 | 1995 | 6 | 4 | 5 | 40 | 36 | 4.2 | 7 | 29.5 |
| 254 | 22 445 | 22 532 | 1995 | 6 | 5 | 21 | 20 | 1995 | 6 | 6 | 11 | 50 | 16.5 | 2 | 6 | 11.8 |
| 254 | 23 624 | 23 779 | 1995 | 6 | 14 | 1 | 50 | 1995 | 6 | 15 | 3 | 40 | 71.5 | 10 | 13 | 130.6 |
| 254 | 27 528 | 27 614 | 1995 | 7 | 11 | 4 | 30 | 1995 | 7 | 11 | 18 | 50 | 32.5 | 5.3 | 15 | 79.2 |
| 254 | 28 274 | 28 394 | 1995 | 7 | 16 | 8 | 50 | 1995 | 7 | 17 | 4 | 50 | 31.5 | 3.9 | 9 | 34.9 |
| 254 | 31 856 | 31 908 | 1995 | 8 | 10 | 5 | 50 | 1995 | 8 | 10 | 14 | 30 | 41.5 | 6.6 | 13 | 85.4 |
| 254 | 34 848 | 34 955 | 1995 | 8 | 31 | 0 | 30 | 1995 | 8 | 31 | 18 | 20 | 35 | 4.7 | 9 | 41.9 |
| 254 | 37 198 | 37 390 | 1995 | 9 | 16 | 8 | 10 | 1995 | 9 | 17 | 16 | 10 | 78 | 10.4 | 13 | 135.3 |
| 254 | 44 763 | 44 792 | 1995 | 11 | 7 | 21 | 0 | 1995 | 11 | 8 | 1 | 50 | 13.5 | 1.8 | 7 | 12.3 |
| 254 | 62 224 | 62 417 | 1996 | 3 | 8 | 3 | 10 | 1996 | 3 | 9 | 11 | 20 | 37 | 4.1 | 4 | 16.4 |
| 254 | 63 300 | 63 352 | 1996 | 3 | 15 | 14 | 30 | 1996 | 3 | 15 | 23 | 10 | 29.5 | 3.6 | 6 | 21.6 |
| 254 | 63 516 | 63 573 | 1996 | 3 | 17 | 2 | 30 | 1996 | 3 | 17 | 12 | 0 | 19 | 2.1 | 3 | 6.4 |
| 254 | 64 235 | 64 291 | 1996 | 3 | 22 | 2 | 20 | 1996 | 3 | 22 | 11 | 40 | 14.5 | 1.6 | 3 | 4.8 |
| 254 | 67 892 | 67 961 | 1996 | 4 | 16 | 11 | 50 | 1996 | 4 | 16 | 23 | 20 | 20.5 | 2.3 | 6 | 14 |
| 254 | 70 595 | 70 663 | 1996 | 5 | 5 | 6 | 20 | 1996 | 5 | 5 | 17 | 40 | 45 | 6 | 10 | 60.4 |
| 254 | 71 164 | 71 231 | 1996 | 5 | 9 | 5 | 10 | 1996 | 5 | 9 | 16 | 20 | 53.5 | 7.1 | 8 | 57.1 |





HESSD
12, 7225–7266, 2015



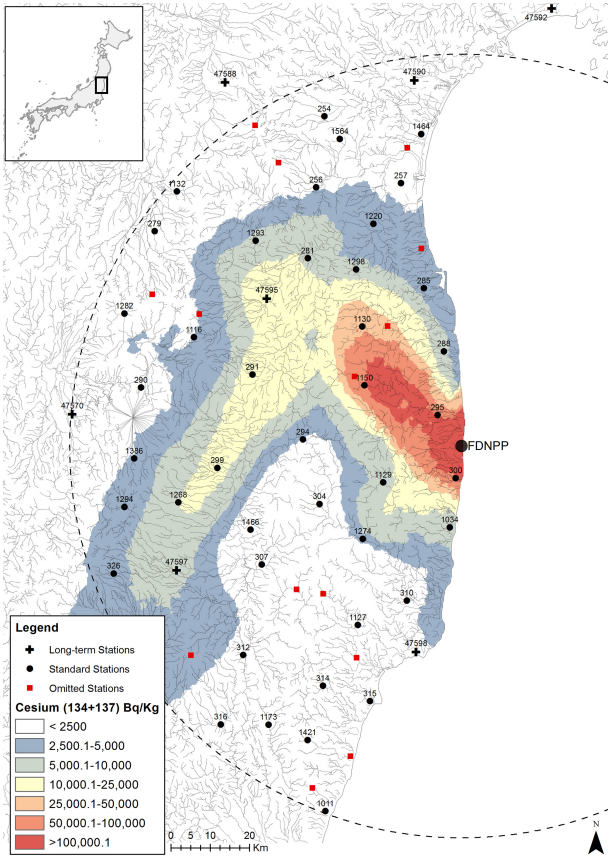


**Figure 1.** Standard, omitted and long-term rainfall stations in the Fukushima region, along with a 100 km buffer around the FDNPP (dashed line) and the radiocesium ($^{134+137}$Cs) fallout plume spatially interpreted from Chartin et al. (2013).





HESSD
12, 7225–7266, 2015



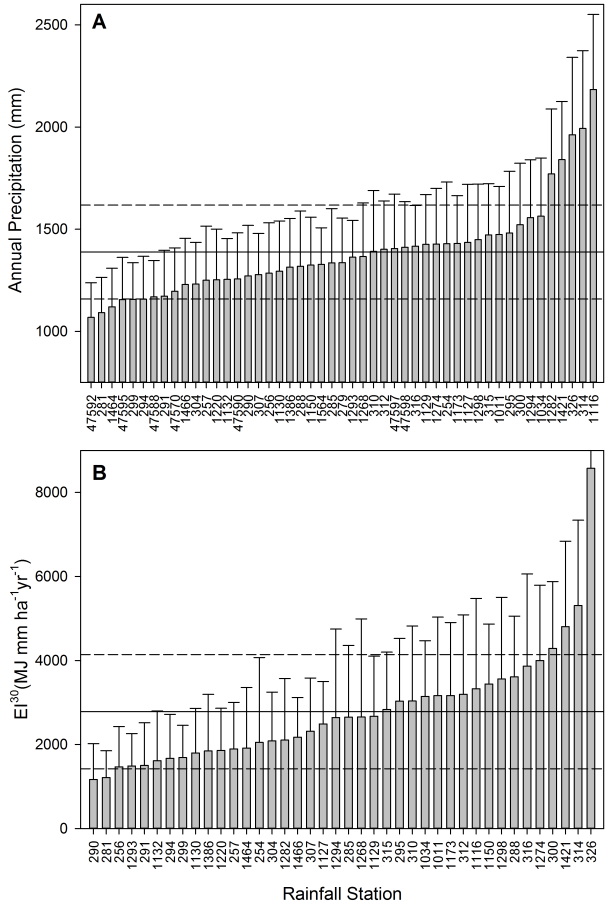


**Figure 2.** Mean annual rainfall (**a** – top) and *R* factor (**b** – bottom) with the solid line representing the mean and the dashed lines being one standard deviation on the mean being the dashed line. The error bars indicate one standard deviation on the mean for individual station.





HESSD
12, 7225–7266, 2015



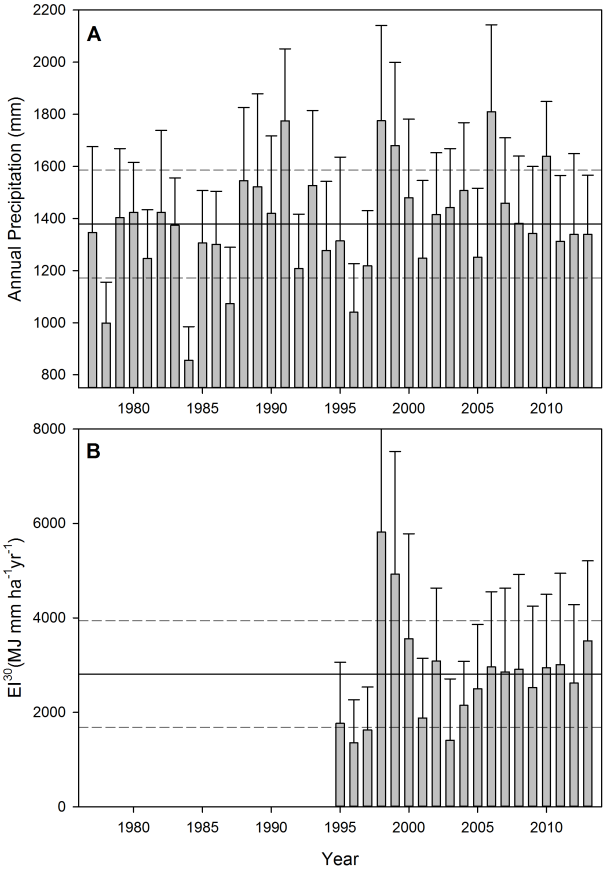


**Figure 3.** Mean annual rainfall (**a** – top) and *R* factor (**b** – bottom) from an average of 45 rainfall stations per year (min 32, max 48) with the solid line representing the mean and the dashed lines representing one standard deviation on the mean. The error bars indicate one standard deviation on the mean for each year.





HESSD
12, 7225–7266, 2015



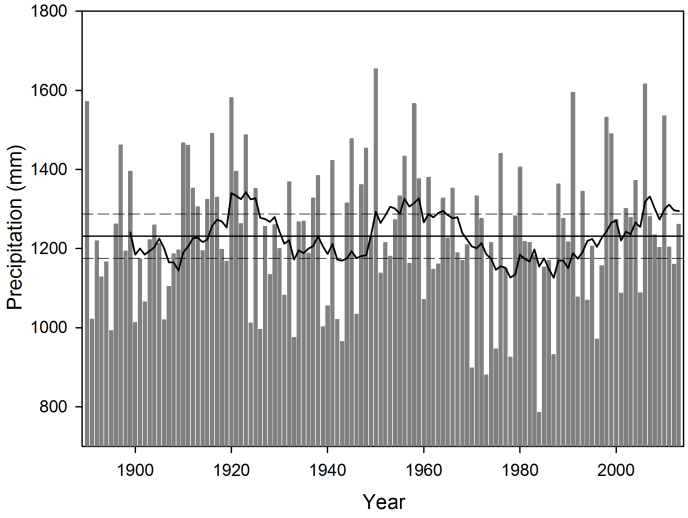


**Figure 4.** Mean annual rainfall from an average of the long-term rainfall stations with the mean annual precipitation (solid line), the standard deviation (dashed line) for the entire period along with the 10 year running average.





HESSD
12, 7225–7266, 2015



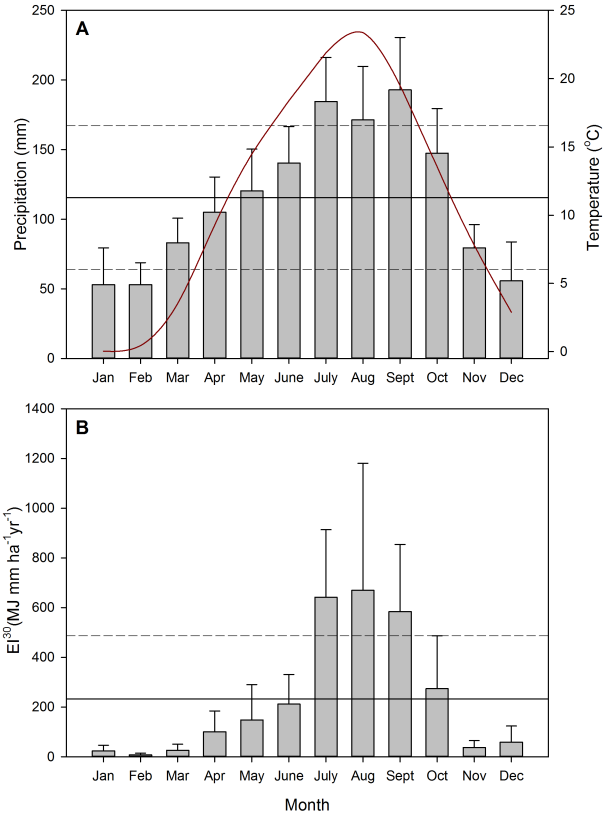


**Figure 5.** Mean monthly rainfall (**a** – top) and *R* factor (**b** – bottom) with error bars indicating one standard deviation on the mean and the solid line representing the monthly mean and dashed lines representing on standard deviation on the mean. The mean monthly temperature is plotted (red line) along with mean monthly rainfall (**a** – top).





HESSD
12, 7225–7266, 2015



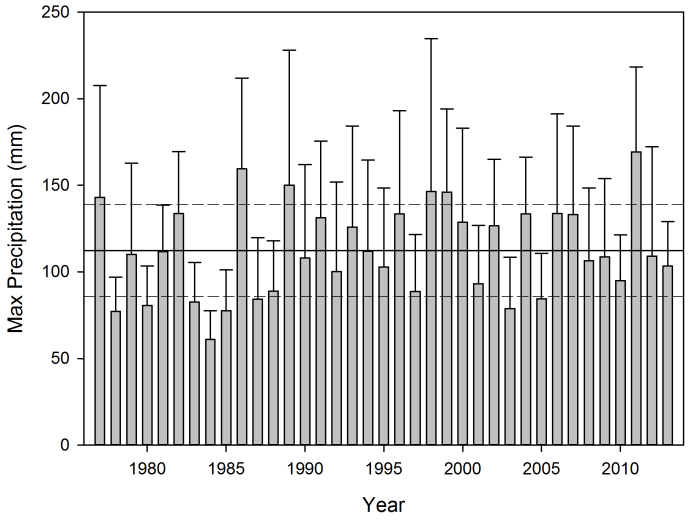


**Figure 6.** Mean maximum daily rainfall from on average of 45 rainfall stations per year (min 32, max 48) with error bars indicating one standard deviation on the mean for each station, along with the mean (solid) and one standard deviation on the mean (dashed line) for the daily rainfall analyses period.





HESSD
12, 7225–7266, 2015



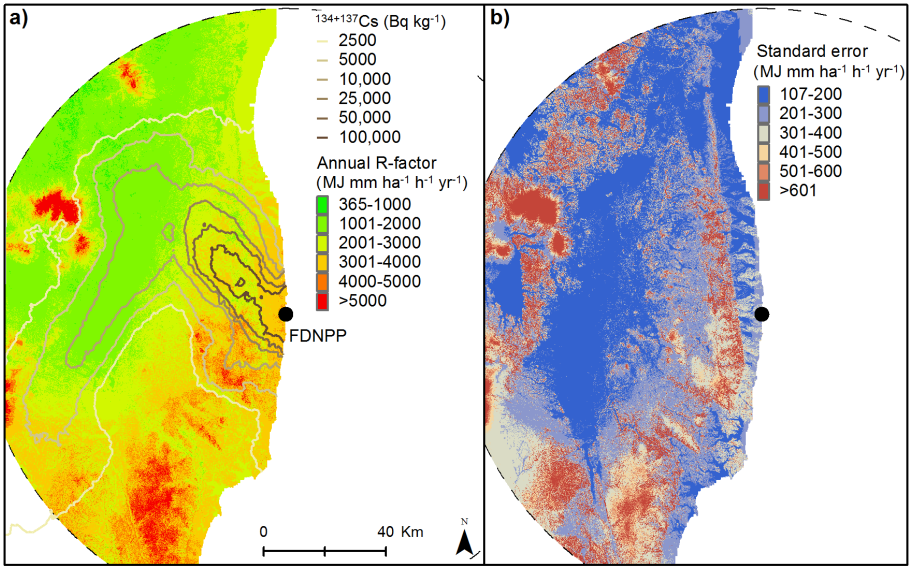


**Figure 7.** Map of annual *R* factor **(a)** and standard errors of the associated model **(b)** for the eastern part of the Fukushima Prefecture. ($^{134+137}$Cs activities in Fig. 6a are decay corrected to 14 June 2011; see Chartin et al. (2013) for details on the method followed to draw this map).





HESSD
12, 7225–7266, 2015



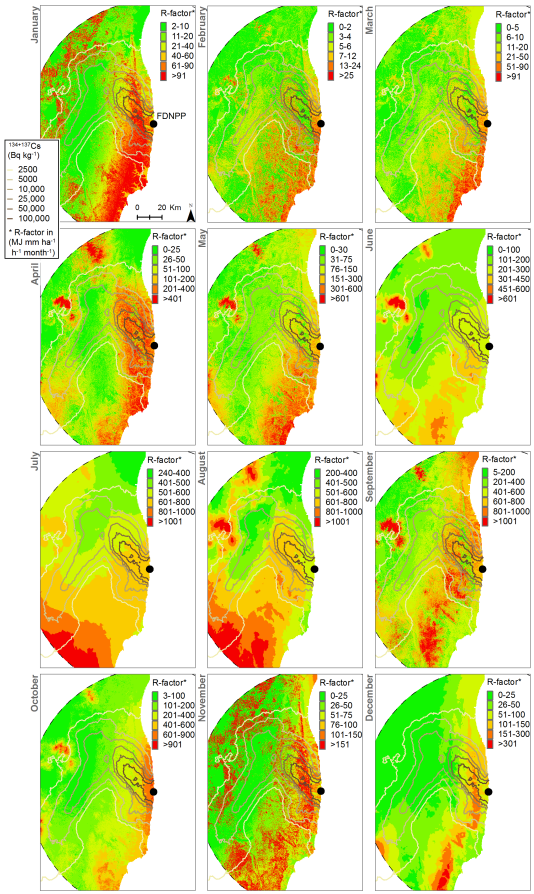


**Figure 8.** Maps of monthly *R* factors for the eastern part of the Fukushima Prefecture ($^{134+137}$Cs activities in Fig. 6a are decay corrected to 14 June 2011; see Chartin et al. (2013) for details on the method followed to draw this map).





HESSD
12, 7225–7266, 2015